

# An upper bound for the directivity index of superdirective acoustic vector sensor arrays

Xijing Guo<sup>a)</sup>

Key Laboratory of Ocean Acoustics and Sensing (Northwestern Polytechnical University),  
Ministry of Industry and Information Technology, Xi'an 710072, China  
xguo@nwpu.edu.cn

Sebastian Miron<sup>b)</sup>

Université de Lorraine, Centre de Recherche en Automatique de Nancy, Unité Mixte de  
Recherche 7039, Vandœuvre-lès-Nancy, F-54506, France  
sebastian.miron@univ-lorraine.fr

Yixin Yang<sup>a)</sup>

Key Laboratory of Ocean Acoustics and Sensing (Northwestern Polytechnical University),  
Ministry of Industry and Information Technology, Xi'an 710072, China  
yxyang@nwpu.edu.cn

Shi'e Yang<sup>a)</sup>

College of Underwater Acoustic Engineering, Harbin Engineering University, 145 Nantong  
Street, 150001 Harbin, China  
yangshie@hrbeu.edu.cn

**Abstract:** Approximate analytical expressions of the white noise gain (WNG) for two superdirective acoustic vector sensor arrays are provided, which disclose the strong dependence of the tradeoff between the WNG and the directivity index (DI) on the highest order of the modes for the pattern synthesis. The considered arrays are a uniform linear array and a uniform circular array. A condition on the WNG that ensures a high array gain in the two-dimensional homogeneous and isotropic noise field is deduced. Using this condition, an upper bound on the highest order of the modes for the pattern synthesis can be derived, and hence the maximum DI can be determined. The presented results are not strictly limited to the two array geometries considered herein, and can be extended to other superdirective acoustic array designs.

© 2016 Acoustical Society of America

[CFG]

Date Received: June 20, 2016      Date Accepted: October 24, 2016

## 1. Introduction

A well-known problem with superdirective arrays is their low white noise gain (WNG), which measures the ability of the array to reject the spatially uncorrelated noise,<sup>1</sup> mainly due to some non-acoustic causes, i.e., the self noise of the sensor (including the electrical noise). As a consequence, the array gain (AG) can be low, despite a high directivity index (DI). To maximize the AG, a tradeoff between the DI and the WNG is necessary.<sup>2,3</sup> The main objective of this letter is to provide an upper bound on the DI for a given miniaturized aperture array, in order to obtain the best AG possible in the 2D homogeneous and isotropic noise field for underwater applications.

For presentation legibility reasons, in this work we restrain ourselves to two miniaturized aperture arrays of 2D particle velocity sensors, i.e., a uniform linear array (ULA)<sup>4</sup> and a uniform circular array (UCA).<sup>5</sup> The so-called 2D particle velocity sensor<sup>4</sup> is an acoustic vector sensor (AVS) composed of only two orthogonally oriented particle velocity sensors. Nevertheless, the obtained results are not necessarily limited to these two configurations and may be extended to other superdirective array geometries, such as the 3-by-3 uniform rectangular array (URA),<sup>6</sup> etc.

## 2. Factors that dominate the white noise gain

### 2.1 The miniaturized-aperture array configurations

We begin with the ULA.<sup>4</sup> This array consists of  $L$  AVSs equally spaced by  $a$  and a pressure sensor positioned at the geometric center of the array, as illustrated by Fig. 1(a). A

<sup>a)</sup>Also at: School of Marine Science and Technology, Northwestern Polytechnical University, Xi'an 710072, China.

<sup>b)</sup>Author to whom correspondence should be addressed.

2D horizontal coordinate system is established with the origin coinciding with the center of the array. The two maximum response axes of the AVSs are aligned either along the  $x$ - or the  $y$ -axis. For simplicity, and without loss of generality, we assume that the sensitivity (scaled by the impedance) of the particle velocity sensors that compose the AVS is equivalent to the sensitivity of the pressure sensor.

Consider a plane wave  $s(t)$ , incident from the azimuthal direction  $\phi$  with wavelength  $\lambda$ , satisfying  $a/\lambda < 1/2\pi$ . Since herein an AVS provides two measurement “channels,” the signal at the output of the AVS ULA can be expressed as a  $(2L + 1) \times 1$  vector

$$\mathbf{x}(t) = \mathbf{a}(\phi)s(t) + \mathbf{n}(t) + \mathbf{u}(t). \quad (1)$$

In this equation, the vector  $\mathbf{a}(\phi)$  denotes the array manifold vector. The other two vectors  $\mathbf{n}(t)$  and  $\mathbf{u}(t)$  denote the contributions of the ambient noise and of the self noise, respectively. The first element of  $\mathbf{x}(t)$  represents the measurements associated with the pressure sensor. The next  $L$  elements give the particle velocity observations made by the  $L$  AVSs along the  $x$ -axis whereas the last  $L$  elements are the observations along the  $y$ -axis.

The  $(2L + 1) \times 1$  vector  $\mathbf{n}(t)$  symbolizes the ambient noise measurements. For the miniaturized-aperture array, the components of ambient noise vector are *correlated* across the sensors.<sup>7</sup> We denote the power of the ambient noise measured at the pressure sensor, say,  $n_1(t)$ , by  $E[|n_1(t)|^2] = \varepsilon^2$ , where  $E(\cdot)$  denotes the expectation operator. Observe that herein, the sensitivity of the sensor has been absorbed in  $\varepsilon^2$ . Consider the simple case where the ambient noise field is 2D homogeneous and isotropic. The power of the ambient noise measured by the  $\ell$ th AVS, along the  $x$  direction, i.e.,  $E[|n_{\ell+1}(t)|^2]$ , and along the  $y$  direction, i.e.,  $E[|n_{\ell+L+1}(t)|^2]$ , can be obtained by simply substituting the elevation angle with  $\pi/2$  into those equations derived for the 3D homogeneous and isotropic noise field,<sup>7</sup> yielding  $E[|n_{\ell+1}(t)|^2] = E[|n_{\ell+L+1}(t)|^2] = \varepsilon^2/2$  for any  $\ell$  in  $1 \leq \ell \leq L$ . In general, the ambient noise power per sensor equals  $\varepsilon^2$ , where a sensor can be either the pressure sensor or an AVS.

In the data model (1), the spatially uncorrelated self noise  $\mathbf{u}(t)$  is separated from the ambient noise. Since the pressure sensor’s contribution to the self noise, i.e., the first element of  $\mathbf{u}(t)$ , is negligible compared to the particle velocity sensors,<sup>8</sup> it is simply set to zero. In addition, we assume that the power of the self noise is identical across all the  $2L$  channels of the AVSs and denoted by  $\sigma^2$ . It should be pointed out that the magnitude of the self noise is independent of the sensitivity of the sensors, which is different from the ambient noise case discussed before. Observe that an AVS of good quality should have high sensitivity and low self noise, implying a large value of  $\varepsilon^2/\sigma^2$ . Thus, in the sequel, the noise ratio  $\varepsilon^2/\sigma^2$  is used as a measure of the “quality” of the AVS.

Let us consider now the UCA illustrated by Fig. 1(b).<sup>5</sup> For comparison purposes, the radius of the UCA is also set to  $a$ . The data model (1) also applies in this case but the array manifold  $\mathbf{a}(\phi)$  is changed. Other than its array geometry, the UCA also differs from the ULA in two main aspects: (i) there is *no* pressure sensor in the

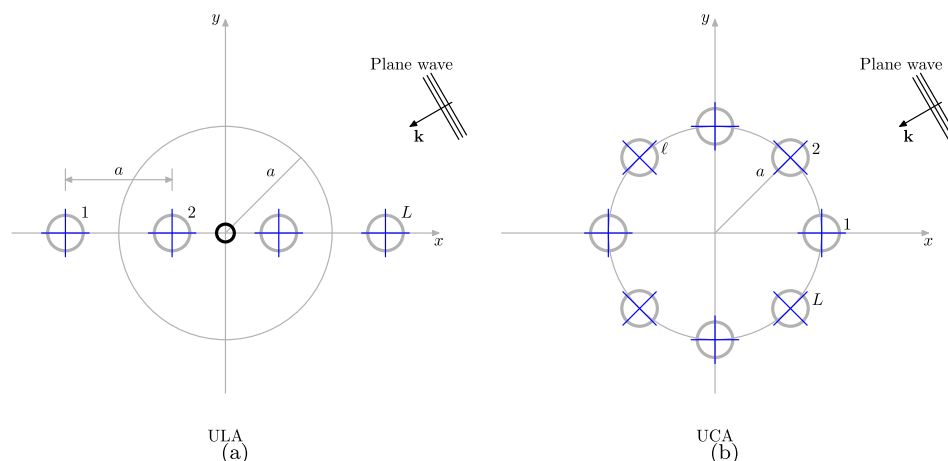


Fig. 1. (Color online) The array geometries of (a) ULA of  $L = 4$  elements and (b) UCA of  $L = 8$  elements, for instance. A gray circle denotes an AVS whereas the smaller dark circle denotes an omnidirectional pressure sensor. The cross on each AVS illustrates the maximum response directions of the two orthogonally oriented particle velocity sensors.

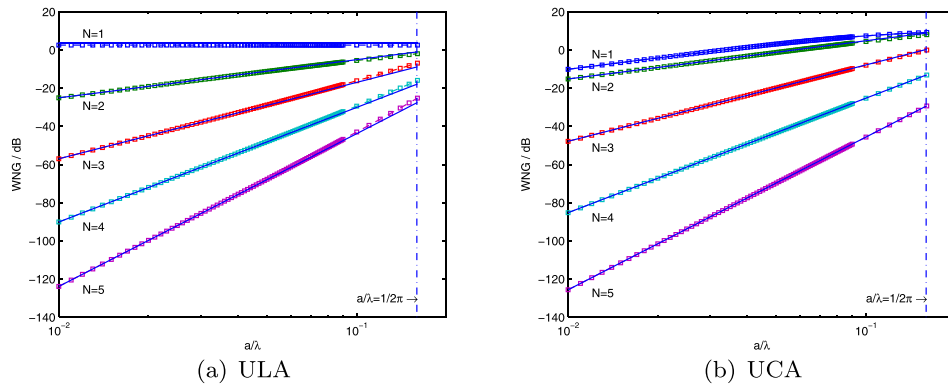


Fig. 2. (Color online) The WNG for the ULA and the UCA. The dashed curves with square markers plot the true values of the WNG (dB), computed numerically, for a steering angle of  $60^\circ$ . The solid curves represent the analytical approximations of the WNG.

UCA, meaning that the dimension of the array response  $\mathbf{x}(t)$  is  $2L \times 1$  and (ii) the two main response axes of the AVSs are aligned along the radial and tangential directions. However, it will be shown in the sequel, that the UCA is still able to produce the same beam pattern as the ULA, with an identical DI.

### 2.2 Directivity index

It is known<sup>9</sup> that the acoustic wavefield can be decomposed into a series of acoustic modes of different orders. For this 2D setup, only the azimuth-dependent components of these modes are considered. Then, each  $n$ th ( $1 \leq n \leq N$ ) order mode has two components  $\cos n\phi$  and  $\sin n\phi$ , where  $N$  is the highest order of these modes. The first step of the modal beamforming extracts the acoustic modes from the planewave measurements. Then, in the second step, the desired beam pattern is synthesized by these modes.

One can observe by comparing Refs. 4 and 5 that, despite their differences in the mode extraction step, the modal beamforming methods for both the ULA and the UCA are very similar in the pattern synthesis stage. Therefore, the same beam pattern can be obtained irrespective of the particular array configuration. Hence, without loss of generality, we choose the desired beam pattern as follows:

$$\mathcal{B}_d(\phi, \varphi) = \frac{1}{2N + 1} \frac{\sin \frac{2N + 1}{2}(\varphi - \phi)}{\sin \frac{1}{2}(\varphi - \phi)}, \quad (2)$$

where  $\varphi$  is the steering angle. For both arrays, one can always find the proper beamformer filter weights  $\mathbf{w}(\varphi)$  such that the practically obtained beam pattern  $\mathcal{B}(\phi, \varphi) = \mathbf{w}(\varphi)^H \mathbf{a}(\phi) \approx \mathcal{B}_d(\phi, \varphi)$ . Then, the DI in the 2D homogenous and isotropic noise field can be calculated as<sup>10</sup>

$$\text{DI} \approx 10 \log_{10} \left[ \frac{1}{2\pi} \int_0^{2\pi} |\mathcal{B}_d(\phi, \varphi)|^2 d\phi \right]^{-1} = 10 \log_{10}(2N + 1). \quad (3)$$

For the AVS ULA, the number of AVSs must be greater than the highest order of the modes,<sup>4</sup> i.e.,  $L \geq N$ . The reason is that the number of AVSs determines the order of the finite differences of the particle velocity observations, which are used to estimate the mode components. Consequently, it determines the highest order of the achievable acoustic modes. For the UCA, however, the requirement on the number of AVSs is given by  $L \geq 2N + 1$ , as a direct consequence of the sampling theorem.<sup>5</sup>

### 2.3 White noise gain

From the definition<sup>10</sup>  $\text{WNG} = -10 \log_{10} \mathbf{w}(\varphi)^H \mathbf{w}(\varphi)$ , we can derive an analytical expression for the WNG of the AVS ULA,<sup>4</sup> given by (in decibels)

$$\text{WNG} \approx 20(N - 1) \log_{10} \frac{2\pi a}{\lambda} + 20 \log_{10} \frac{2N + 1}{2^N} \frac{(N - 1)!}{\sqrt{(2N - 2)!}}. \quad (4)$$

Clearly, it is closely dependent on two factors, i.e., the relative inter-sensor spacing  $a/\lambda$  and the highest order of the modes for the pattern synthesis  $N$ .

Analogously, the WNG of the AVS UCA can be approximately expressed as<sup>5</sup>

$$\text{WNG} \approx \begin{cases} -10 \log_{10} \left( 2 + \frac{\lambda}{2\pi a} \right) + 10 \log_{10} L + 20 \log_{10} \frac{3}{2}, & N = 1; \\ 20 \log_{10} \frac{2\pi a}{\lambda} + 10 \log_{10} L + 20 \log_{10} \frac{5}{6}, & N = 2; \\ 20(N-1) \log_{10} \frac{2\pi a}{\lambda} + 10 \log_{10} \frac{L}{2} + 20 \log_{10} \frac{2N+1}{2^N} \frac{1}{(N-1)!}, & N \geq 3. \end{cases} \quad (5)$$

It is clear, by comparing Eq. (5) with Eq. (4), that a third factor also influences the WNG of the UCA, i.e., the number of AVSs  $L$ . A mild benefit of about 3 dB can be obtained by doubling the number of AVSs in the UCA.

In addition, we observe by comparing the analytical expressions of the WNG (4) and (5) with the expression of the DI (3), that there is only one common factor in these equations, i.e., the highest order of the modes for the pattern synthesis  $N$ . This factor governs the tradeoff between the WNG and the DI: the DI increases with  $N$  whereas the WNG decreases.

#### 2.4 Numerical validation of the analytical WNG expressions

In this subsection, the analytical expressions (4) and (5) will be validated numerically. We consider five cases where the highest order of the modes  $N$  varies from 1 to 5. In each case, both arrays produce the same beam patterns, with identical DIs. Since the ULA needs at least  $N$  AVSs to extract the modes up to the  $N$ th order and it does not benefit from any extra AVS,<sup>4</sup> the number of AVSs that form the ULA is fixed to  $L=5$ . However, for the UCA, the necessary number of AVSs is  $L \geq 2N+1$ , and a higher WNG can be achieved if additional sensors are available. Even though we set the number of AVSs composing the UCA to be the minimum necessary, i.e.,  $L=11$ , the UCA still has more than twice as many AVSs as the ULA. This makes the comparison unfair to some extent. However, this is negligible since the influence of the number  $L$  of AVSs on the WNG of the UCA is rather insignificant compared with the influence of the other two factors, i.e.,  $a/\lambda$  and  $N$ .

We examine the WNG of the AVS ULA first. The steering angle is set to  $60^\circ$ . The WNG is computed numerically versus the relative inter-sensor spacing  $a/\lambda$ , as shown in Fig. 2(a). On the plots, the upper bound of  $a/\lambda$  is set to  $1/2\pi$ , which ensures a DI invariant of  $a/\lambda$ . The approximate analytical expression (4) is also compared with the numerically computed WNG values, showing a very good agreement. In the case of  $N=1$ , only one AVS is actually used. Therefore, the WNG is naturally independent of the relative inter-sensor spacing  $a/\lambda$ .

It is obvious, from the well separated curves in Fig. 2(a), that the WNG varies significantly with the highest order of the modes for the pattern synthesis  $N$ , as if it “jumped” with  $N$ . This means that the WNG can be increased drastically (by tens of dB) by merely reducing  $N$  by 1, especially when  $a/\lambda \ll 1/2\pi$ .

Figure 2(b) plots the analytical expression of the WNG (5) versus  $a/\lambda$  in comparison with its numerically computed values for the AVS UCA. The plots are very close to each other, which validates Eq. (5). Moreover, by comparing Fig. 2(b) with Fig. 2(a), we observe that the UCA has similar WNGs to the ULA. The only difference occurs when  $N=1$ . In this case, unlike the ULA, observations from all 11 AVSs of the UCA contribute to the extraction of the first order acoustic mode. Hence, the WNG of the UCA in the case  $N=1$  is also dependent on the relative inter-sensor spacing  $a/\lambda$ .

### 3. The upper bound

The array gain (AG) for a superdirective array, under the 2D homogeneous and isotropic noise field assumption, can be expressed in terms of the DI and the WNG as<sup>6</sup>

$$\frac{1}{10^{\text{AG}/10}} \approx \frac{1}{10^{\text{DI}/10}} + \left( \frac{\sigma}{\varepsilon} \right)^2 \frac{1}{10^{\text{WNG}/10}}. \quad (6)$$

For superdirective arrays, the WNG is much less than 0 dB when  $a/\lambda \ll 1$ . Therefore, the value of AG is smaller than that of DI. A high DI may not necessarily result in a

high AG, but it sets an upper bound on the AG. It is obvious from Eq. (6) that  $AG \approx DI$ , if and only if

$$10 \log_{10} \frac{\varepsilon^2}{\sigma^2} + WNG \gg DI. \quad (7)$$

For superdirective arrays composed of high-quality AVSs, the quantity  $10 \log_{10}(\varepsilon^2/\sigma^2)$  is large. In addition, since  $a/\lambda \ll 1/2\pi$ , the absolute value of the WNG is much larger than the DI. Hence, by neglecting the DI, Eq. (7) reduces to

$$WNG \gg -10 \log_{10} \frac{\varepsilon^2}{\sigma^2}. \quad (8)$$

Otherwise, if  $AG \ll DI$ , it holds that

$$AG \approx 10 \log_{10} \frac{\varepsilon^2}{\sigma^2} + WNG \ll DI. \quad (9)$$

Furthermore, if in Eq. (9) we set  $AG = 0$  dB, then we have

$$WNG \approx -10 \log_{10} \frac{\varepsilon^2}{\sigma^2}. \quad (10)$$

This provides a lower bound on the WNG that ensures  $AG > 0$  dB.

Therefore, an upper bound for the highest order of the modes for the pattern synthesis  $N$  can be derived by substituting the WNG in Eq. (10) by Eqs. (4) and (5) for the AVS ULA and the UCA, respectively. Since the WNG varies significantly with  $N$ , the optimum value of  $N$  can be found slightly smaller than this upper bound. Consequently, the maximum DI of the superdirective array can be determined by Eq. (3).

#### 4. Examples

In this section, numerical examples are provided to show how the maximum DI can be found. Figure 3(a) illustrates the simulation results of the WNG versus the DI for the AVS ULA. The four folded curves correspond to four different values of the relative inter-sensor spacing  $a/\lambda$  that vary from 0.01 to 0.1, sampled uniformly with a step of 0.03. From Fig. 3(a), we can observe that the WNG decreases sharply with the DI. The left ends of these curves converge to the same point, where the value of the DI reads 4.8 dB. This corresponds to the case  $N=1$  where only one among the five AVSs is used for beamforming. In this case, the WNG is invariant with  $a/\lambda$ , as it was shown in Fig. 2(a).

The AG, as a function of the WNG and the DI, is also shown by the color plots. Herein, the noise ratio is fixed to  $10 \log_{10} \varepsilon^2/\sigma^2 = 60$  dB. A clear border can be observed which divides the image into two parts. In the upper part of the figure (the colored part), the AG is above 0 dB, whereas in the lower part, which is left blank, the AG is less than 0 dB. This border is also associated to the case  $WNG \approx -10 \log_{10} \varepsilon^2/\sigma^2$ . Then, the highest AG is achievable above this border, i.e., the domain  $WNG > -10 \log_{10} \varepsilon^2/\sigma^2$ . For instance, consider the case where  $a/\lambda = 0.04$ . Figure 3(a) shows that at the third point (from left to right, i.e.,  $N=3$ ) among the five on the tradeoff curve, the highest AG is achieved, which gives the optimum DI

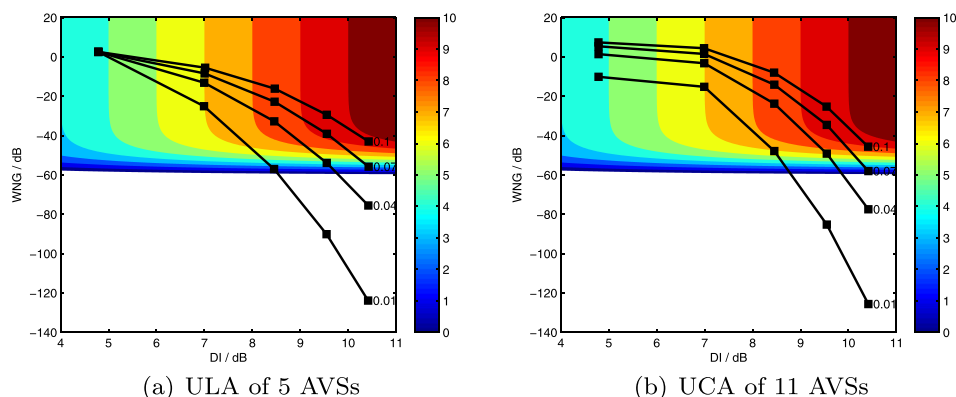


Fig. 3. (Color online) Tradeoff between DI and WNG compared with AG. The digits on the right end of each curve are the relative inter-sensor spacings used for the simulations.

of nearly 8.5 dB. Meanwhile, the upper bound on the DI, given by the point on that tradeoff curve closet to the border curve, is about 9.5 dB ( $N=4$ ).

The simulation results for the AVS UCA at the same four values of the relative inter-sensor spacing  $a/\lambda$  are presented in Fig. 3(b). The results are similar to those of the ULA case in general, except that the tradeoff curves are not converging at their left ends, where  $N=1$ . This is still because the WNG of the AVS UCA is dependent on  $a/\lambda$  for  $N=1$ . By analogy, we conjecture that these results, derived for the ULA and UCA cases, also apply to other superdirective arrays, such as the URA.<sup>6</sup>

## 5. Conclusions

In this letter, analytical expressions for the WNG of the ULA (Ref. 5) and the UCA (Ref. 4) of AVSs are presented for the case where the relative sensor spacing  $a/\lambda \ll 1/2\pi$ . These analytical expressions highlight the strong dependence of the tradeoff between WNG and DI on the highest order of the modes for the pattern synthesis  $N$ . From a simple relation that links the AG to the DI and to the WNG, we derive a condition on the WNG (10) which provides an upper bound for  $N$ . The optimum  $N$ , which maximizes the AG, is slightly below this upper bound, and hence determines the maximum DI. It is also shown that both arrays can achieve identical DIs, and therefore they have similar WNGs and AGs. Based on the similar behaviors of the two arrays, we conjecture that most results of this letter can be straightforwardly extended to other AVS superdirective array configurations.

## Acknowledgments

This work was supported by the National Natural Science Foundation of China under Grants Nos. 11304251 and 11527809, and the Specialized Research Fund for the Doctoral Program of Higher Education of China under Grant No. 20136102120014. The authors would like to thank Professor Jingdong Chen for his valuable suggestions.

## References and links

- <sup>1</sup>S. Doclo and M. Moonen, "Superdirective beamforming robust against microphone mismatch," *IEEE Trans. Audio Speech Lang. Process.* **15**(2), 617–631 (2007).
- <sup>2</sup>H. Cox, R. M. Zeskind, and T. Kooij, "Practical supergain," *IEEE Trans. Acoust. Speech Sign. Process.* **34**(3), 393–398 (1986).
- <sup>3</sup>J. Chen, J. Benesty, and C. Pan, "On the design and implementation of linear differential microphone arrays," *J. Acoust. Soc. Am.* **136**(6), 3097–3113 (2014).
- <sup>4</sup>B. Gur, "Particle velocity gradient based acoustic mode beamforming for short linear vector sensor arrays," *J. Acoust. Soc. Am.* **135**(6), 3463–3473 (2014).
- <sup>5</sup>N. Zou and A. Nehorai, "Circular acoustic vector-sensor array for mode beamforming," *IEEE Trans. Sign. Process.* **57**(8), 3041–3052 (2009).
- <sup>6</sup>X. Guo, S. Yang, and S. Miron, "Low-frequency beamforming for a miniaturized aperture three-by-three uniform rectangular array of acoustic vector sensors," *J. Acoust. Soc. Am.* **138**(6), 3873–3883 (2015).
- <sup>7</sup>M. Hawkes and A. Nehorai, "Acoustic vector-sensor correlations in ambient noise," *IEEE J. Ocean. Eng.* **26**(3), 337–347 (2001).
- <sup>8</sup>G. L. D'Spain, J. C. Luby, G. R. Wilson, and R. A. Gramann, "Vector sensors and vector sensor line arrays: Comments on optimal array gain and detection," *J. Acoust. Soc. Am.* **120**(1), 171–185 (2006).
- <sup>9</sup>L. E. Kinsler, A. R. Frey, A. B. Coppens, and J. V. Sanders, *Fundamentals of Acoustics*, 4th ed. (Wiley, New York, 2000), Chap. 5, pp. 113–148.
- <sup>10</sup>H. L. Van Trees, *Optimum Array Processing* (Wiley, New York, 2002), Chap. 2, pp. 17–89.